

MERANet: Facial Micro-Expression Recognition using 3D Residual Attention Network

Viswanatha Reddy Gajjala*
IIIT Sri City
viswanatha.g15@iiits.in

Sai Prasanna Teja Reddy*
The University of Chicago
bogireddyteja@uchicago.edu

Snehasis Mukherjee
Shiv Nadar University
snehasis.mukherjee@snu.edu.in

Shiv Ram Dubey
IIIT Sri City
srdubey@iiits.in

Abstract

We propose a facial micro-expression recognition model using 3D residual attention network called MERANet. The proposed model takes advantage of spatial-temporal attention and channel attention together, to learn deeper fine-grained subtle features for classification of emotions. The proposed model also encompasses both spatial and temporal information simultaneously using the 3D kernels and residual connections. Moreover, the channel features and spatio-temporal features are re-calibrated using the channel and spatio-temporal attentions, respectively in each residual module. The experiments are conducted on benchmark facial micro-expression datasets. A superior performance is observed as compared to the state-of-the-art for facial micro-expression recognition.

1. Introduction

In recent years, facial expression recognition using deep learning techniques have gained lot of popularity among the research community because of its potential applications across various fields, such as psychology, marketing, security, etc. However, recognizing true human emotions from facial expressions often becomes unreliable due to the performer's deliberate control on the expressions, depending on the social circumstances. Hence, micro-expression recognition is evolved as an attempt to capture the true emotion of a performer [2]. Micro-expressions are involuntarily exposed short term expressions that appear during an active suppression of facial expression to hide the true emotion. Micro-expressions are very short spanned (fraction of a second), which makes the task of capturing the relevant features for recognizing emotion as challenging [3].

*Both authors have equally contributed

Efforts have been made to apply Convolutional Neural Networks (CNNs) for micro-expression recognition [24, 33]. Although CNN models are able to automatically capture useful features from the videos, but they are often unable to capture the minute textural changes on various parts of face, observed during micro-expressions. To capture the minute textural information, facial landmarks are used for feature extraction [10]. However, temporal features are also important in recognizing facial micro-expressions.

A few efforts have also been made in capturing temporal cues from optical flow, for recognizing micro-expressions [17, 4, 16]. However, optical flow often suffers from unnecessary motion information from background pixels. Another line of thought for capturing temporal features suggests applying a Long Short Term Memory (LSTM) on the spatial features [12, 13, 11]. A few 3D CNN based models can also be found in the literature, to capture temporal cues [29, 18]. The existing approaches of applying temporal features often fails to capture the minute texture information from micro-expression videos, where the expression continues for the very short span of time. Attention based models often show efficacy in extracting the minute texture information [23, 14]. However, attention mechanism is still not properly explored for micro-expression recognition task. Wang *et al.* proposed a spatial attention model for micro-expression recognition [35]. However, to capture the temporal information from the short span of video, where the micro-expression takes place, we propose a 3D channel and spatio-temporal attentions based model called as MERANet. The main contributions of this paper are as follows:

- A 3D residual attention is introduced here for recognizing subtle features related to micro-expressions by attention guided re-calibration of features.
- In order to prioritize the important channels and spatio-temporal features, the channel attention and spatio-

temporal attention blocks are used as part of the residual module.

- The increase in number of parameters in the proposed model is negligible as compared to the base model.
- Extensive experiments are performed to show the impact of the proposed 3D residual attention model on micro-expression recognition. We show the saliency map to visualize the effect the proposed approach.

2. Literature Review

2.1. Facial Micro-Expression Recognition

The facial micro-expression recognition methods can be categorized into two classes, including the handcrafted feature based methods and deep learning based methods.

2.1.1 Handcrafted Feature based Methods

The traditional approaches for micro-expression recognition were mostly focused on superficial attributes involving complex calculations. Polikovsky [27] proposed a three step algorithm that divides the facial region into twelve parts to extract facial cubes. They computed 3D orientation histogram descriptor to capture correlations across the frames for each cube. They classified the expression based on the normalized descriptor vectors. Shreve *et al.* [31] utilized the facial strain caused by the non-rigid motion of facial muscles during an expression. The magnitude of strain was found using optical flow over different regions of the face. Pfister *et al.* [26] used temporal interpolation model to address variable video length problem. They introduced spatiotemporal local texture descriptors to generate feature vector and finally, various kinds of classifiers have been tried to classify the micro-expression. Huang *et al.* [8] proposed a spatiotemporal completed local quantized pattern that extracts sign, magnitude and orientation components from an expression and constructed a codebook for each component that holds more dynamic pattern representations. Liu *et al.* [19] proposed a method that generates a compact feature vector by finding main directional mean optical flow using optical flow field over different regions of interest. The final feature vector is fed into SVM to classify micro-expressions. Zhao *et al.* [43] proposed a computationally compact feature using Local Binary Pattern - Three Orthogonal Planes (LBP-TOP) which can efficiently extract co-occurring features from neighboring points. Lu *et al.* [21] proposed a fusion based feature that finds differentials of optical flow over horizontal and vertical components. The fused feature vector is fed into an SVM classifier for classification.

2.1.2 Deep Learning based Methods

In most of the computer vision applications, the deep learning techniques outperform the handcrafted feature based methods due to its increased feature learning capability from the data [15]. Patel *et al.* [24] proposed a deep learning model for micro-expression recognition, where they used transfer learning to initialize the CNN with weights of a CNN trained on largely available macro-expression data to avoid overfitting. Takalkar implemented a variety of data augmentation techniques to generate synthetic data, resembling different environments to deal with lack of training data. Finally a CNN is applied to classify micro-expressions [33]. Qiuyu *et al.* [17] proposed a three step algorithm where a multi-task CNN was used to find the facial landmarks. Deep CNN was used to calibrate the optical flow features from different facial regions. Finally, an SVM was employed to classify the micro-expressions. Liong *et al.* [4] collected the optical flow feature for each micro-expression and used it as input to a CNN for classification. Li *et al.* [16] proposed a 3D flow based CNN that uses gray scale images along with components of optical flow in different directions as input to classify micro-expressions. Wang *et al.* [35] proposed an image based residual model that uses micro-attention units and transfer learning to classify micro-expressions. The model fails to consider temporal information across the frames, which is important for micro-expression videos. Several proposals can be found in the literature [12, 13, 11] that used two step architecture where, a CNN is applied on each frame of the micro-expression video to generate spatial features and then a Long Short Term Memory (LSTM) based Recurrent Neural Network (RNN) is used to learn the temporal inter-dependencies between different spatial features from previous step. Reddy *et al.* [29] proposed a 3D CNN based model that tries to capture both spatial and temporal information in a micro-expression video simultaneous using 3D kernels. Liong *et al.* [18] proposed a shallow triple stream 3D CNN that uses optical strain, horizontal and vertical flows from the onset and apex frames to classify micro-expressions.

The existing methods focus neither on the minute spatial changes on face regions during micro-expressions nor the temporal cues, as the micro-expressions last for a small span of time. An attention mechanism can help to overcome this.

2.2. Attention Mechanism

Human perception process is based on the attention mechanism [23]. Human vision obtains the target area that needs to be focused on, and pays more attention on the target area to obtain more detailed information that helps to capture the visual structure of the target better [14]. Attention mechanism is used to find the region of interest within an image and to highlight the representation of the region of interest [9]. The two main aspects of attention mechanism

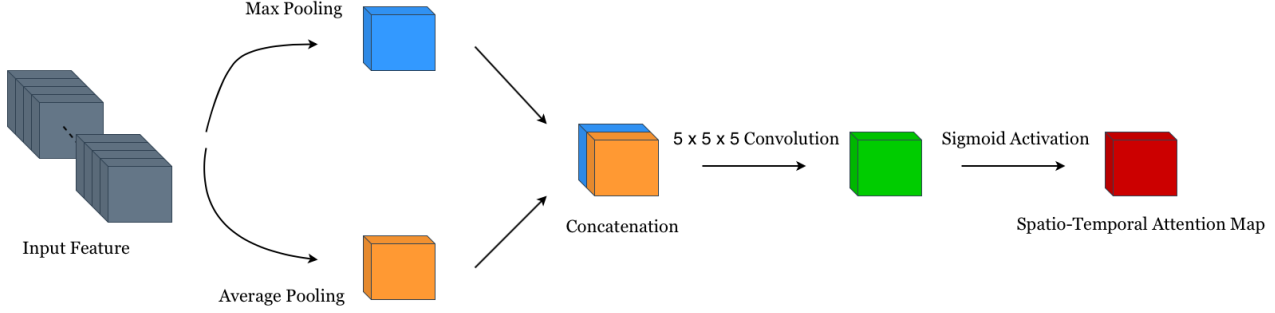


Figure 1. The proposed Spatial-Temporal attention block.

in deep learning are (a) to obtain the meaningful channels for the respective input feature and (b) to pay attention to the most informative channels to obtain the salient locations.

Recently, several studies applied attention mechanism to enhance the performance of CNNs in a range of visual tasks, such as image classification, image localization and video understanding [1, 32]. Wang *et al.* [36] proposed Residual Attention Network (RAN) which uses a trunk-and-mask module to incorporate an attention mechanism. By re-weighting the feature map, the network not only performs well but is also robust to input noise. Hu *et al.* [7] introduced Squeeze-and-Excitation module to exploit the inter-channel relationship. Adding to this, Woo *et al.* [37] introduced spatial attention to further improve the image classification performance. In [25], Peng *et al.* designed an attention branch that helps to spotlight finger micro-gesture and reduces the noise introduced from the background and wrist. The spatial attention has improved the recognition accuracy by 3%. However the attention block proposed in that study increased the parameters by about $2M$. Similarly for micro-expression recognition, attention mechanism helps the model to focus on the face and facial regions and suppress the irrelevant facial areas and background.

The existing attention works have not utilized the 3D channel and spatio-temporal attentions, which are important in the context of facial micro-expression recognition. In this work, we design a novel and effective 3D residual attention mechanism to simultaneously learn fine and subtle features along spatial, temporal and channel dimensions. The proposed attention modules, including channel attention and spatio-temporal attention, add few parameters leading to minimal computation overhead.

3. Proposed MERANet Model for Facial Micro-Expression Recognition

Given a facial micro-expression video, our objective is to obtain a good representation in terms of their emotional score. We propose a deep learning model, named MERANet, for micro-expression recognition using 3D residual

attention network. The proposed residual attention (RA) network is constructed by stacking up multiple RA blocks. The RA block comprises of two major sub-modules: (a) A Spatio-Temporal Attention module to extract the spatio-temporal importance map and (b) A Channel Attention module to extract more discriminative features by prioritizing the important channels.

3.1. Spatio-Temporal Attention Module

We compute the spatio-temporal attention map by utilizing the spatial-temporal relationship among the features. The spatio-temporal attention focuses on where we need to pay more attention in the input feature volume.

In order to compute the spatio-temporal attention without increasing the model parameters, we first apply average-pooling and max-pooling operations along the channel axis and aggregate them by concatenating to generate an efficient feature descriptor $\mathcal{F}^{st} \in \mathcal{R}^{2 \times T' \times W' \times H'}$, where T' , W' and H' represent the temporal dimension, width, and height respectively, of the generated feature descriptor. The pooling operation is employed along the channel axis as it is effective in highlighting the informative regions [41]. The average pooling across the channels is defined as,

$$\mathcal{F}_{avg}^{st}(1, t, h, w) = \frac{1}{C'} \sum_{c=1}^{C'} F_{c,t,h,w}, \quad (1)$$

and the max pooling across the channels is defined as,

$$\mathcal{F}_{max}^{st}(1, t, h, w) = \max_{c \in \{1, 2, \dots, C'\}} (F_{c,t,h,w}), \quad (2)$$

where $t \in \{1, 2, \dots, T'\}$, $h \in \{1, 2, \dots, H'\}$, and $w \in \{1, 2, \dots, W'\}$, $F \in \mathcal{R}^{C' \times T' \times W' \times H'}$ corresponds to the input feature volume and C' is the number of channels in the input feature (F).

In order to limit the module complexity, a single convolution operation is performed on the feature descriptor to produce a more refined feature map followed by a sigmoid activation function. The final generated attention importance map (\mathcal{A}^{st}) learns the importance score for each

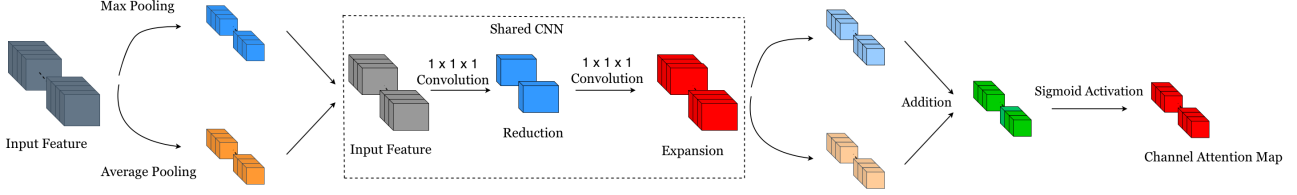


Figure 2. The proposed Channel Attention mechanism.

spatial-temporal location. The \mathcal{A}^{st} is defined as,

$$\mathcal{A}^{st} = \sigma[W_{5 \times 5 \times 5}(\mathcal{F}^{st})], \quad (3)$$

where \mathcal{F}^{st} is given as,

$$\mathcal{F}^{st} = \text{Concat}(\mathcal{F}_{avg}^{st}; \mathcal{F}_{max}^{st}), \quad (4)$$

and $\text{Concat}(\mathcal{F}_{avg}^{st}; \mathcal{F}_{max}^{st}) \in \mathcal{R}^{2 \times T' \times W' \times H'}$ is the concatenated features of average pooling and max pooling across the channel dimension, $\mathcal{A}^{st} \in \mathcal{R}^{1 \times T' \times W' \times H'}$ is the generated attention importance map, σ denotes the sigmoid function and $W_{5 \times 5 \times 5}$ corresponds to a convolution operation with the kernel of size 5 with *same* padding. Note that all the values in the importance map are in the range 0 to 1, thus mimicking the probability of being important. Basically, \mathcal{A}^{st} encodes that which spatio-temporal information to emphasize or suppress. The block diagram of the spatio-temporal attention module is shown in Fig. 1. Element-wise multiplication is employed between the input feature volume and the spatio-temporal importance map (\mathcal{A}^{st}) to re-weight each pixel value and obtain the refined feature map. The re-calibrated feature activation (F^{st}) is defined as,

$$F_c^{st} |_{\forall c \in \{1, 2, \dots, C'\}} = F_c \otimes \mathcal{A}^{st}, \quad (5)$$

where F_c and F_c^{st} are the c^{th} channel of input and re-calibrated output using spatio-temporal attention and \otimes denotes the element-wise multiplication.

3.2. Channel Attention Block

The spatio-temporal attention captures the weight for each spatio-temporal feature volume. However, it is not able to distinguish the weight among the different channels of feature volume. Thus, we also propose a channel attention block in the residual framework. The channel features in the CNNs are exploited extensively to extract more discriminative features. We compute a channel attention map by utilizing the inter-channel relationship of features. The channel attention map focuses on finding the meaningful channels for the respective input feature volume. Integrating a channel attention map helps to improve the learning ability of the model by re-calibrating the channels of the input feature volume with increased or decreased weight. In order to capture the channel attention effectively for a feature volume ($\mathcal{F}' \in \mathcal{R}^{C' \times T' \times W' \times H'}$), first we squeeze the

spatial and temporal dimensions of the input feature volume by applying average pooling and max pooling and then we combine the squeezed features by concatenating them.

The average pooling over spatial and temporal dimensions is given as,

$$\mathcal{F}_{avg}^{ch}(c, 1, 1, 1) = \frac{1}{T' \times W' \times H'} \sum_{t=1}^{T'} \sum_{h=1}^{H'} \sum_{w=1}^{W'} \mathcal{F}'(c, t, h, w), \quad (6)$$

and the max pooling over spatial and temporal dimensions are given as,

$$\mathcal{F}_{max}^{ch}(c, 1, 1, 1) = \max_t \max_h \max_w \mathcal{F}'(c, t, h, w), \quad (7)$$

where $t \in \{1, 2, \dots, T'\}$, $h \in \{1, 2, \dots, H'\}$, $w \in \{1, 2, \dots, W'\}$, $\mathcal{F}_{avg}^c \in \mathcal{R}^{C' \times 1 \times 1 \times 1}$, $\mathcal{F}_{max}^c \in \mathcal{R}^{C' \times 1 \times 1 \times 1}$, $c \in \{1, 2, \dots, C'\}$, and C' is the number of channels.

The channel descriptors \mathcal{F}_{max}^{ch} and \mathcal{F}_{avg}^{ch} are then fed to a shared sub-network to fully capture the inter-dependencies. We propose two design choices for the shared sub-network. One variant is with the convolutional layers and other with the multi-layer perceptron layers (MLP). Our experimental results show that the shared network with convolutions is better than the MLP. The detailed analysis will follow in experimental results in Section 4. The shared convolutional network consists of a convolution layer with the channel reduction mechanism (through $1 \times 1 \times 1$ convolution) to reduce the computation overhead. The ReLU activation is used to introduce the non-linearity followed by a dimension increasing layer to match the input channel dimension (through $1 \times 1 \times 1$ convolution).

The final channel attention map (\mathcal{A}^{ch}) is computed as,

$$\mathcal{A}^{ch} = \sigma[W_e(\varphi(W_s(\mathcal{F}_{avg}^{ch}))) + W_e(\varphi(W_s(\mathcal{F}_{max}^{ch})))], \quad (8)$$

where σ and φ correspond to the Sigmoid and ReLU activation functions, respectively, W_s and W_e are the convolution operations in the shared network with $W_s(\cdot) \in \mathcal{R}^{\frac{C'}{r} \times 1 \times 1 \times 1}$ and $W_e(\cdot) \in \mathcal{R}^{C' \times 1 \times 1 \times 1}$, r is the channel reduction ratio in the shared sub-network, and $\mathcal{A}^{ch} \in \mathcal{R}^{C' \times 1 \times 1 \times 1}$. The reduction ratio(r) is set to 16 in this paper.

Note that all the values in the channel importance map are in the range 0 to 1. Thus, it represents the probability of being important for each channel. The block diagram of the channel attention module is shown in Fig. 2.

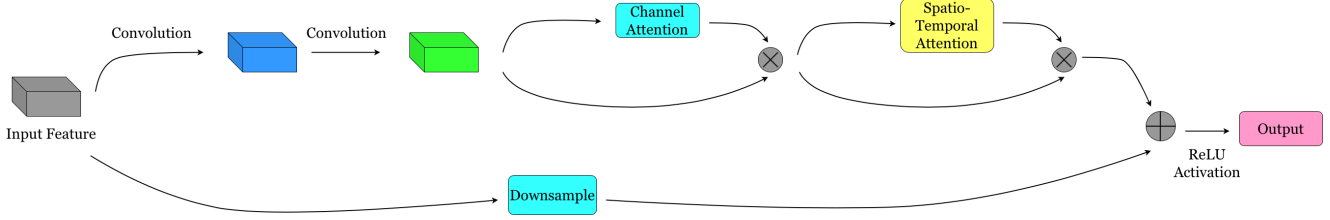


Figure 3. The proposed 3D residual attention module by integrating the 3D convolutions, channel attention and spatio-temporal attention blocks.

Channel-wise multiplication is employed between the input feature volume and the channel importance map (\mathcal{A}^c) to obtain the re-calibrated channels of the output feature map. The re-calibrated feature activation (F'_{ch}) is computed as,

$$F'_{ch}(c, t, h, w) = F'(c, t, h, w) \otimes \mathcal{A}^{ch}(c, 1, 1, 1), \quad (9)$$

for $\forall c \in \{1, 2, \dots, C'\}$, $\forall t \in \{1, 2, \dots, T'\}$, $\forall h \in \{1, 2, \dots, H'\}$, and $\forall w \in \{1, 2, \dots, W'\}$, where F' and F'_{ch} are the input and re-calibrated output using channel attention, respectively.

3.3. Residual Attention Module

In this paper, we propose a 3D RA module by utilizing the spatio-temporal and channel attention blocks. In contrast to usual residual block, we introduce the attention blocks into the residual module. The residual attention module comprises of two 3D convolution operations, channel attention, spatial-temporal attention, residual connection followed by an activation function. For simplicity, we ignore the batch-norm and activation layers in the block diagram.

The block diagram for the proposed 3D RA module is shown in Fig. 3. Suppose $\mathcal{I} \in \mathcal{R}^{C \times T \times W \times H}$ is the input feature volume to the proposed residual attention module and $\mathcal{I}^{conv} \in \mathcal{R}^{C' \times T' \times W' \times H'}$ is the generated intermediate feature volume after two convolution blocks. We apply the channel attention operation over \mathcal{I}^{conv} to generate the channel attention map \mathcal{A}^{ch} as defined in Eq. (8) which uses the average pooling and max pooling over spatial and temporal dimensions as given in Eq. (6) and (7), respectively. The re-calibrated intermediate feature after channel attention is given using Eq. (9) as,

$$\mathcal{I}^{ch} = \mathcal{I}^{conv} \otimes \mathcal{A}^{ch}. \quad (10)$$

Next, we apply the spatio-temporal attention operation over \mathcal{I}^{ch} to generate the spatio-temporal attention map \mathcal{A}^{st} as defined in Eq. (3) which uses the average pooling and max pooling across channel dimension as given in Eq. (1) and (2), respectively. The re-calibrated intermediate feature after spatio-temporal attention is given using Eq. (5) as,

$$\mathcal{I}^{st} = \mathcal{I}^{ch} \otimes \mathcal{A}^{st}. \quad (11)$$

The channel attention excites the important channels separately, whereas the spatio-temporal attention excites the important spatio-temporal features. The last step in the proposed residual module is to add the generated re-calibrated features with the original input of this block. The final output of the proposed residual module ($\mathcal{O} \in \mathcal{R}^{C' \times T' \times W' \times H'}$) is computed as,

$$\mathcal{O} = \varphi[\mathcal{I}^{st} + d(\mathcal{I})] \quad (12)$$

where φ is the ReLU activation function and d is a down-sampling function to change the dimension of input from $C \times T \times W \times H$ to $C' \times T' \times W' \times H'$. The down-sampling function is used in the residual path to match the dimensions of the features \mathcal{I}^{st} and \mathcal{I} . (a) If the dimensions of the \mathcal{I}^{st} and \mathcal{I} are same then the down-sampling will be a simple identity mapping with no additional parameters added. (b) If the dimensions of the \mathcal{I}^{st} and \mathcal{I} are different then the down-sampling function will use $1 \times 1 \times 1$ convolution with the stride 2 to match the dimensions.

3.4. Network Architecture

The residual network (ResNet) and its variants are one of the most successful architectures for image classification [6] [38] [42]. A basic residual module consists of two convolutional layers in a sequence. The first convolutional layer is followed by a batch normalization and a ReLU activation, whereas the second convolution layer is followed by a batch normalization. The residual module adds the output of the second convolution layer to the input which is followed by a ReLU activation function. The ResNet uses the residual connections that enforces the network to learn the difference of transformation instead of complete transformation. It facilitates better gradient flow during the back-propagation and helps in the optimization of the network. Thus, facilitating the training of very deep networks feasible. Due to the residual property, the ResNet abates the vanishing gradient problem.

We also generate the proposed MERANet architecture by following the ResNet architecture in this work. The MERANet-18 is constructed by stacking up the multiple 3D residual attention modules. We use the identity connections and zero padding in the residual paths of the residual attention module to avoid increasing the number of parameters

of the model. The 3D residual attention modules are used as the basic building blocks of the proposed MERANet model. We add a stem network to get the reasonable size feature map similar to the ResNet. We also employ a fully connected layer at the end to classify the emotion score. The detailed architecture is summarized in supplementary.

4. Experimental Settings

In this section, first we provide a brief description of three benchmark micro-expression datasets used for the experiments, followed by the pre-processing details and the training settings.

4.1. Micro-Expression Datasets Used

We have used three benchmark micro-expression datasets to evaluate the proposed model, namely CASMEI, CASMEII, and CAS(ME)².

CASME I Dataset [40]: CASME I dataset is divided into two parts: CASME A and CASME B, which are constructed under two different conditions. CASME A contains images with 1280×720 resolution under natural light settings. Whereas, CASME B contains images with resolution of 640×480 under the artificial light settings. Both settings have a temporal resolution of 60 fps. Altogether, CASME dataset contains 195 micro-expressions belonging to seven different classes. For this experiment, we have chosen three classes, including disgust (34 samples), repression (36 samples), and tense (45 samples) based on the higher number of samples in these classes.

CASME II Dataset [39]: CASME II is a spontaneous micro-expressions dataset built under well-controlled laboratory environment. The samples have a higher face resolution at 280×340 pixels and a relatively high temporal resolution (200 fps). The database has five micro-expression categories. The number of samples for each category is distributed unequally (there are 60 samples for disgust and only 7 samples for sadness). Since the data is not uniformly distributed across the classes to obtain consistent results, we have used three classes, including disgust (63 sample), happy (32 samples), and surprise (28 samples) based on the higher number of samples in these classes.

CAS(ME)² Dataset [28]: CAS(ME)² dataset comprises of both macro-expressions and micro-expressions. This dataset is constructed by showing 9 elicitation videos to 22 participants under artificial light settings. The elicitation videos contain three emotions (happy, angry, and disgust) evoking videos. CAS(ME)² contains the samples with 640×480 resolution at 30 frames per second. In our experiment, we have only used micro-expressions of CAS(ME)² dataset. The used dataset contains three expressions, namely happy (18 samples), angry (22 samples), and disgust (17 samples).

4.2. Pre-Processing

In the experiments, first, we select the apex frame in the video corresponding to the micro-expression in order to generate a training sample. As the data is captured at different frame rates per second, we have assigned temporal depth for CASMEI and CASMEII as 32 and CAS(ME)² as 16. Also, we have considered samples having atleast 16 frames for CASMEI and CASMEII in this experimentation. A 16-frame clip is generated around the selected apex frame. If the video is shorter than 16 frames, then we replicate the edge frames as many times as necessary. The temporal dimension is selected based on the average number of frames available in a video clip. We spatially resize the sample to 112×112 pixels. The size of each sample is 3 channels \times 16 frames \times 112 pixels \times 112 pixels, and each sample is horizontally flipped with 0.5 probability. Mean subtraction is applied for each sample by subtracting the mean values from the sample for each channel. Each sample is normalized by the standard deviation.

4.3. Training Settings

We have performed 75%-25% train-test split for CASME I and CASME II and 80%-20% train-test split for CAS(ME)² due to less samples. Among the splits 80% of data is used as a training set and the rest is used as a validation set. Stratified sampling is used for the validation split to maintain consistency across the results. The train-validation split-up is performed once and then the same training and validation sets are used for all the experiments.

The weights of both convolutional and fully-connected layers are initialized with the Xavier initialization proposed in [5]. We set the parameter to random values uniformly drawn from $[-rv, rv]$, where rv is defined as, $rv = \sqrt{\frac{6}{(d_{in} + d_{out})}}$ where d_{in} and d_{out} are the size of input and output channels, respectively. All biases are initialized to 0. For batch normalization layers, weights are initialized to 1.

The optimizer proposed in [22] is used for training. We use Categorical Cross Entropy as the loss function. Each model is trained for 100 epochs with a batch size of 8. The learning rate is initialized to 0.1. Learning rate adjustment is one of the crucial steps while training. We use the cosine annealing strategy proposed in [20]. The cosine annealing decreases the learning rate from the initial value to 0 by following the cosine function. The intuition behind using annealing is that it helps to traverse quickly from the initial parameters to a range of good parameter values with a smaller learning rate. Thus, we can explore the deeper and narrower parts of the loss function, which potentially improves the training progress by avoiding the divergence.

Table 1. The performance of the proposed MERANet model in terms of the facial micro-expression recognition accuracy as compared to the existing state-of-the-art models. Note that the results of existing methods are taken from the respective papers. The HCM and DLM denote the hand crafted method and deep learning method, respectively.

Method	CASME I	CASME II	CAS(ME) ²	Year	Method Type
STCLQP [8]	57.31 %	58.39 %	-	2016	HCM
FMBH [21]	61.33 %	69.11 %	73.67 %	2018	HCM
CNN + Optical Flow [17]	56.60 %	56.94 %	-	2018	DLM
3D Flow CNN [16]	54.44 %	59.11 %	-	2018	DLM
LEARNet [34]	80.62 %	76.57 %	76.57 %	2019	DLM
MicroExpSTCNN [29]	-	-	87.80 %	2019	DLM
MicroAttention [35]	-	65.90 %	-	2020	DLM
3D Residual Network (Ours)	81.0%	83.3 %	83.3 %	—	DLM
MERANet (Proposed Model)	90.5 %	91.7 %	91.7 %	—	DLM

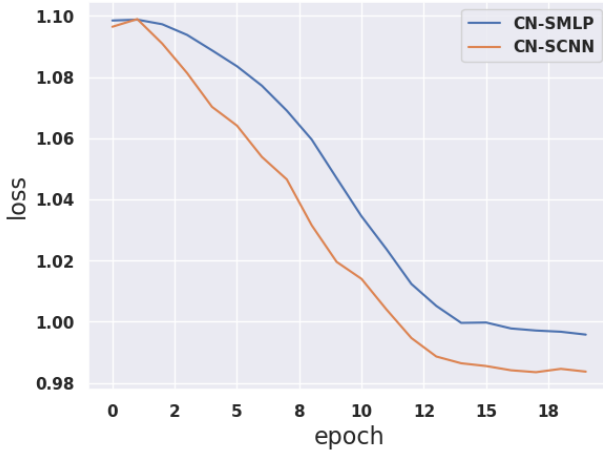


Figure 4. Validation loss curves for the shared network choices, including channel attention using shared multi-layer perceptron (CN-SMLP) and channel attention using shared convolutional neural network (CN-SCNN).

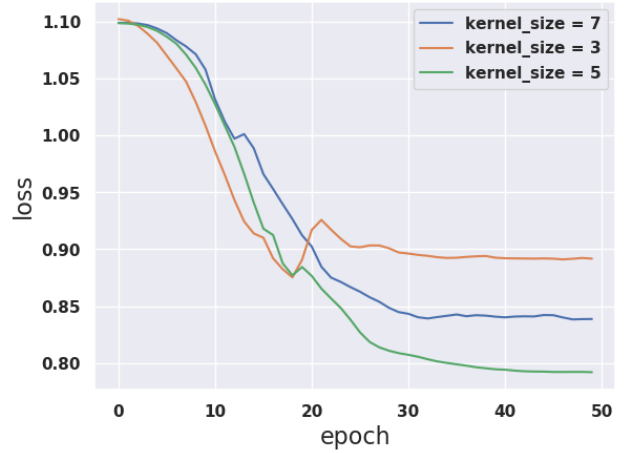


Figure 5. The impact of kernel size on the spatio-temporal attention block to prioritize the spatio-temporal information in the intermediate features. The plots are shown for the kernel size of 3, 5 and 7. Medium kernel size is better suited.

5. Results and Discussion

In this section, first we present the experimental results comparison, then the impact of kernel size on spatio-temporal attention module and the visualization of impact of attention through saliency maps.

5.1. Experimental Results

Experiments are done by training both the 3D residual network and the proposed 3D residual attention network models. The results are compared in terms of the facial micro-expression recognition accuracy. The performance of the proposed residual attention network is compared with the state-of-the-art hand-crafted methods (HCM) and deep learning methods (DLM) as shown in Table 1. The results are computed over three benchmark facial micro-expression datasets, including CASME I, CASME II and CAS(ME)². Note that the results of competing methods are taken from the corresponding papers. It is noticed from the results in

Table 1 that the proposed MERANet model outperforms the existing hand crafted and deep learning models with a great margin. As expected, the channel attention and the spatio-temporal attention blocks help the residual network to learn better micro-level spatio-temporal features leading to the enhanced decision making for facial micro-expression recognition.

The total number of parameters for the original 3D ResNet model is 3,31,67,811 and the total number of parameters for our proposed 3D MERANet model is 3,35,47,552. However, only 3,79,741 parameters are added to the MERANet which is 0.01% extra compared to the 3D ResNet. So, the overall overhead added by the proposed attention module is negligible in terms of both parameters and computation. The quantitative results from Table 1 show the effectiveness of our proposed attention modules.

5.2. Impact of Shared Network in Channel Attention

In this subsection, we show the comparison between the shared CNN and shared MLP in channel attention. For this study, we use the $CAS(ME)^2$ dataset. In-order to fully capture the interrelationship, the channel descriptor of average pooling \mathcal{F}_{avg}^{ch} and max pooling \mathcal{F}_{max}^{ch} are fed to a shared network. In this subsection, we experimentally verify the proposed two design choices of shared networks, i.e., (a) Channel Attention with shared convolutional neural network (CN-SCNN) and (b) Channel Attention with shared multilayer perceptron (CN-SMLP).

Both the design choices are trained under the same settings. We observe that the residual attention model with shared CNN in the channel attention module work well compared to the model with the shared MLP in the shared network. Shared CNN works on the sliding window concept (which focuses on local regions of interest), whereas shared MLP works on the global feature connections. Due to the aforementioned property, shared CNN goes hand in hand with the attention module by improving the learning capability of the model. The loss curves for both the design choices are plotted in Fig. 4. From the validation loss curve in Fig. 4, we observe that the CN-SCNN outperforms the CN-SMLP at every epoch. Model trained with the CN-SCNN module converges faster compared to the model trained with the CN-SMLP. In conclusion, we infer that the shared CNN in the channel attention module is a better design choice compared to the shared MLP.

5.3. Impact of Kernel Size on Spatio-Temporal Attention

The performance of spatial-temporal attention block is mainly dependant on the applied convolution operation. In general, convolution layer performance depends on the size of the filter used. The kernel size plays a prominent role in extracting the subtle features. So, we have experimented with different kernel sizes, i.e., 3, 5, and 7 to find the optimal kernel size that boosts the model learning capability. The validation curve is shown in Fig. 5 having the plots corresponding to each kernel size. It is observed that the smaller kernel size (i.e., small receptive field) doesn't help the model to learn better. In contrast, higher kernel size ($k = 7$) increases the computation head, yet it fails to generalize better. From Fig. 5, we also infer that a reasonable receptive field is needed for deciding important regions. In the comparison of different convolution kernel sizes, we find the kernel size of 5 helps the model to learn better micro-expression representation.

5.4. Impact of Attention Through Saliency Map

In this subsection, we empirically show the effectiveness of our proposed model. For this study, we use all the

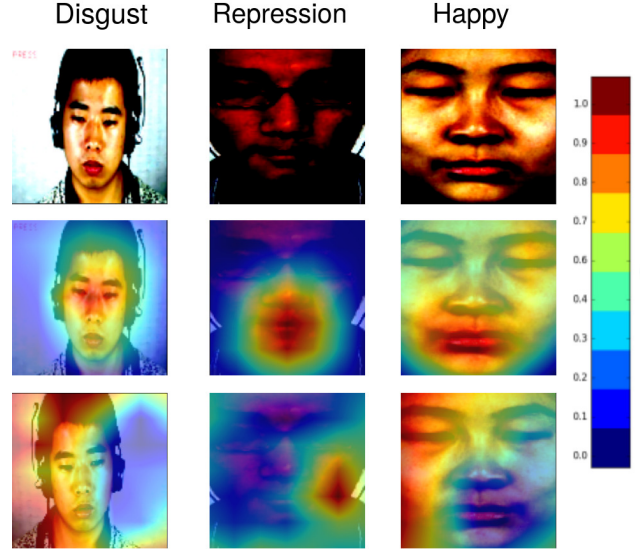


Figure 6. Comparison between the saliency visualizations of the proposed MERANet (Attention) with 3D ResNet (No Attention). The 1st row depicts the input image, the 2nd row contains saliency visualizations from the proposed model and the last row contains the saliency visualizations from the 3D ResNet model. The ground-truth label is shown on the top of each input image.

three datasets. In order to further understand the behavior of the proposed model, we have used the feature visualization technique proposed in [30]. These feature visualizations help us to find which spatial locations trigger the classification outcome, thus providing the insights about the model's understanding of the emotions. The feature visualizations are given in Fig. 6. According to [3], an emotion depicting disgust on a subject's face has facial muscle movements centered around the nose of the subject. Similarly, a happy emotion has facial muscle movements centered around the lip region. From Fig. 6, we infer that the MERANet focuses on the face regions completely ignoring the background. Furthermore, it gives more weight to facial regions corresponding to an emotion. The saliency maps of 3D ResNet model seem to be very arbitrary by considering the noisy regions in the decision making process. Whereas, the saliency maps for the proposed MERANet model clearly matches the intuition with the general procedure of finding facial expressions and more convincing.

6. Conclusion

We have introduced a 3D residual attention based MERANet model for micro-expression recognition. The proposed 3D residual attention module utilizes the benefits of channel attention as well as spatio-temporal attention. These attention blocks help the proposed model to focus over the spatio-temporal features leading to the facial micro-expression recognition. We have conducted the ex-

tensive experiments with the proposed model over three benchmark datasets and compared with the state-of-the-art models. The proposed MERANet model outperforms the existing models with a negligible increase in the number of parameters. We also found that the shared CNN is better suitable with channel attention. However, the kernel size of 5 is better suitable with spatio-temporal attention. The saliency map of the proposed MERANet model is very close to the human perception of the emotions in terms of the facial features contribution towards the identification of the emotions.

References

- [1] C. Cao, X. Liu, Y. Yang, Y. Yu, J. Wang, Z. Wang, Y. Huang, L. Wang, C. Huang, W. Xu, et al. Look and think twice: Capturing top-down visual attention with feedback convolutional neural networks. In *Proceedings of the IEEE international conference on computer vision*, pages 2956–2964, 2015.
- [2] P. Ekman. Lie catching and microexpressions. *The philosophy of deception*, 1(2):5, 2009.
- [3] R. Ekman. *What the face reveals: Basic and applied studies of spontaneous expression using the Facial Action Coding System (FACS)*. Oxford University Press, USA, 1997.
- [4] Y. Gan, S.-T. Liong, W.-C. Yau, Y.-C. Huang, and L.-K. Tan. Off-apexnet on micro-expression recognition system. *Signal Processing: Image Communication*, 74:129–139, 2019.
- [5] X. Glorot and Y. Bengio. Understanding the difficulty of training deep feedforward neural networks. In *Proceedings of the thirteenth international conference on artificial intelligence and statistics*, pages 249–256, 2010.
- [6] K. He, X. Zhang, S. Ren, and J. Sun. Deep residual learning for image recognition. In *Proceedings of the IEEE conference on computer vision and pattern recognition*, pages 770–778, 2016.
- [7] J. Hu, L. Shen, and G. Sun. Squeeze-and-excitation networks. In *Proceedings of the IEEE conference on computer vision and pattern recognition*, pages 7132–7141, 2018.
- [8] X. Huang, G. Zhao, X. Hong, W. Zheng, and M. Pietikäinen. Spontaneous facial micro-expression analysis using spatiotemporal completed local quantized patterns. *Neurocomputing*, 175:564–578, 2016.
- [9] L. Itti and C. Koch. Computational modelling of visual attention. *Nature reviews neuroscience*, 2(3):194–203, 2001.
- [10] G. Jelena, C. Milica, M. Marina, N. Angelina, D. Hasan, and A. Gholamreza. Automatic hidden sadness detection using micro-expressions. In *12th IEEE International Conference on Automatic Face and Gesture Recognition (FG 2017)*. IEEE.
- [11] H.-Q. Khor, J. See, R. C. W. Phan, and W. Lin. Enriched long-term recurrent convolutional network for facial micro-expression recognition. In *2018 13th IEEE International Conference on Automatic Face & Gesture Recognition (FG 2018)*, pages 667–674. IEEE, 2018.
- [12] D. H. Kim, W. J. Baddar, J. Jang, and Y. M. Ro. Multi-objective based spatio-temporal feature representation learning robust to expression intensity variations for facial expression recognition. *IEEE Transactions on Affective Computing*, 10(2):223–236, 2017.
- [13] D. H. Kim, W. J. Baddar, and Y. M. Ro. Micro-expression recognition with expression-state constrained spatio-temporal feature representations. In *Proceedings of the 2016 ACM on Multimedia Conference*, pages 382–386. ACM, 2016.
- [14] H. Larochelle and G. E. Hinton. Learning to combine foveal glimpses with a third-order boltzmann machine. In *Advances in neural information processing systems*, pages 1243–1251, 2010.
- [15] Y. LeCun, Y. Bengio, and G. Hinton. Deep learning. *Nature*, 521(7553):436–444, 2015.
- [16] J. Li, Y. Wang, J. See, and W. Liu. Micro-expression recognition based on 3d flow convolutional neural network. *Pattern Analysis and Applications*, 22(4):1331–1339, 2019.
- [17] Q. Li, J. Yu, T. Kurihara, and S. Zhan. Micro-expression analysis by fusing deep convolutional neural network and optical flow. In *2018 5th International Conference on Control, Decision and Information Technologies (CoDIT)*, pages 265–270. IEEE, 2018.
- [18] S.-T. Liong, Y. Gan, J. See, H.-Q. Khor, and Y.-C. Huang. Shallow triple stream three-dimensional cnn (ststnet) for micro-expression recognition. In *2019 14th IEEE International Conference on Automatic Face & Gesture Recognition (FG 2019)*, pages 1–5. IEEE, 2019.
- [19] Y.-J. Liu, J.-K. Zhang, W.-J. Yan, S.-J. Wang, G. Zhao, and X. Fu. A main directional mean optical flow feature for spontaneous micro-expression recognition. *IEEE Transactions on Affective Computing*, 7(4):299–310, 2015.
- [20] I. Loshchilov and F. Hutter. Sgdr: Stochastic gradient descent with warm restarts. *arXiv preprint arXiv:1608.03983*, 2016.
- [21] H. Lu, K. Kpalma, and J. Ronsin. Motion descriptors for micro-expression recognition. *Signal Processing: Image Communication*, 67:108–117, 2018.
- [22] J. Ma and D. Yarats. On the adequacy of untuned warmup for adaptive optimization. *arXiv preprint arXiv:1910.04209*, 2019.
- [23] V. Mnih, N. Heess, A. Graves, et al. Recurrent models of visual attention. In *Advances in neural information processing systems*, pages 2204–2212, 2014.
- [24] D. Patel, X. Hong, and G. Zhao. Selective deep features for micro-expression recognition. In *2016 23rd international conference on pattern recognition (ICPR)*, pages 2258–2263. IEEE, 2016.
- [25] M. Peng, C. Wang, and T. Chen. Attention based residual network for micro-gesture recognition. In *2018 13th IEEE International Conference on Automatic Face & Gesture Recognition (FG 2018)*, pages 790–794. IEEE, 2018.
- [26] T. Pfister, X. Li, G. Zhao, and M. Pietikäinen. Recognising spontaneous facial micro-expressions. In *2011 international conference on computer vision*, pages 1449–1456. IEEE, 2011.
- [27] S. Polikovskiy, Y. Kameda, and Y. Ohta. Facial micro-expressions recognition using high speed camera and 3d-gradient descriptor. In *3rd International Conference on*

Imaging for Crime Detection and Prevention (ICDP 2009), pages 1–6. IET, 2009.

- [28] F. Qu, S.-J. Wang, W.-J. Yan, and X. Fu. Cas (me) 2: A database of spontaneous macro-expressions and micro-expressions. In *International Conference on Human-Computer Interaction*, pages 48–59. Springer, 2016.
- [29] S. P. T. Reddy, S. T. Karri, S. R. Dubey, and S. Mukherjee. Spontaneous facial micro-expression recognition using 3d spatiotemporal convolutional neural networks. In *2019 International Joint Conference on Neural Networks (IJCNN)*, pages 1–8. IEEE, 2019.
- [30] R. R. Selvaraju, M. Cogswell, A. Das, R. Vedantam, D. Parikh, and D. Batra. Grad-cam: Visual explanations from deep networks via gradient-based localization. In *Proceedings of the IEEE international conference on computer vision*, pages 618–626, 2017.
- [31] M. Shreve, S. Godavarthy, D. Goldgof, and S. Sarkar. Macro and micro-expression spotting in long videos using spatiotemporal strain. In *IEEE International Conference on Face and Gesture (FG 2011)*, pages 51–56. IEEE, 2011.
- [32] S. K. Sønderby, C. K. Sønderby, L. Maaløe, and O. Winther. Recurrent spatial transformer networks. *arXiv preprint arXiv:1509.05329*, 2015.
- [33] M. A. Takalkar and M. Xu. Image based facial micro-expression recognition using deep learning on small datasets. In *2017 international conference on digital image computing: techniques and applications (DICTA)*, pages 1–7. IEEE, 2017.
- [34] M. Verma, S. K. Vipparthi, G. Singh, and S. Murala. Learnet: Dynamic imaging network for micro expression recognition. *IEEE Transactions on Image Processing*, 29:1618–1627, 2019.
- [35] C. Wang, M. Peng, T. Bi, and T. Chen. Micro-attention for micro-expression recognition. *Neurocomputing*, 410:354–362, 2020.
- [36] F. Wang, M. Jiang, C. Qian, S. Yang, C. Li, H. Zhang, X. Wang, and X. Tang. Residual attention network for image classification. In *Proceedings of the IEEE conference on computer vision and pattern recognition*, pages 3156–3164, 2017.
- [37] S. Woo, J. Park, J.-Y. Lee, and I. So Kweon. Cbam: Convolutional block attention module. In *Proceedings of the European conference on computer vision (ECCV)*, pages 3–19, 2018.
- [38] S. Xie, R. Girshick, P. Dollár, Z. Tu, and K. He. Aggregated residual transformations for deep neural networks. In *Proceedings of the IEEE conference on computer vision and pattern recognition*, pages 1492–1500, 2017.
- [39] W.-J. Yan, X. Li, S.-J. Wang, G. Zhao, Y.-J. Liu, Y.-H. Chen, and X. Fu. Casme ii: An improved spontaneous micro-expression database and the baseline evaluation. *PloS one*, 9(1):e86041, 2014.
- [40] W.-J. Yan, Q. Wu, Y.-J. Liu, S.-J. Wang, and X. Fu. Casme database: a dataset of spontaneous micro-expressions collected from neutralized faces. In *2013 10th IEEE international conference and workshops on automatic face and gesture recognition (FG)*, pages 1–7. IEEE, 2013.
- [41] S. Zagoruyko and N. Komodakis. Paying more attention to attention: Improving the performance of convolutional neural networks via attention transfer. *arXiv preprint arXiv:1612.03928*, 2016.
- [42] S. Zagoruyko and N. Komodakis. Wide residual networks. *arXiv preprint arXiv:1605.07146*, 2016.
- [43] G. Zhao and M. Pietikainen. Dynamic texture recognition using local binary patterns with an application to facial expressions. *IEEE transactions on pattern analysis and machine intelligence*, 29(6):915–928, 2007.

Supplementary Material

Table 2 shows the network architecture of the proposed MERANet model.

Table 2. Network Architecture of the proposed MERANet model.

Block/Layer Name	MERANet	Output Size
stem	$3 \times 7 \times 7$, BN, ReLU	$64 \times 16 \times 56 \times 56$
RA-block 1.1	$3 \times 3 \times 3$, BN, ReLU $3 \times 3 \times 3$, BN, Channel Attention, ST Attention, ReLU	$64 \times 16 \times 56 \times 56$
RA-block 1.2	$3 \times 3 \times 3$, BN, ReLU $3 \times 3 \times 3$, BN, Channel Attention, ST Attention, ReLU	$64 \times 16 \times 56 \times 56$
RA-block 2.1	$3 \times 3 \times 3$, BN, ReLU $3 \times 3 \times 3$, BN, Channel Attention, ST Attention, downsample($1 \times 1 \times 1$, stride = $2 \times 2 \times 2$, BN) ReLU	$128 \times 8 \times 28 \times 28$
RA-block 2.2	$3 \times 3 \times 3$, BN, ReLU $3 \times 3 \times 3$, BN, Channel Attention, ST Attention, ReLU	$128 \times 8 \times 28 \times 28$
RA-block 3.1	$3 \times 3 \times 3$, BN, ReLU $3 \times 3 \times 3$, BN, Channel Attention, ST Attention, downsample($1 \times 1 \times 1$, stride = $2 \times 2 \times 2$, BN) ReLU	$256 \times 4 \times 14 \times 14$
RA-block 3.2	$3 \times 3 \times 3$, BN, ReLU $3 \times 3 \times 3$, BN, Channel Attention, ST Attention, ReLU	$256 \times 4 \times 14 \times 14$
RA-block 4.1	$3 \times 3 \times 3$, BN, ReLU $3 \times 3 \times 3$, BN, Channel Attention, ST Attention, downsample($1 \times 1 \times 1$, stride = $2 \times 2 \times 2$, BN) ReLU	$512 \times 2 \times 7 \times 7$
RA-block 4.2	$3 \times 3 \times 3$, BN, ReLU $3 \times 3 \times 3$, BN, Channel Attention, ST Attention, ReLU	$512 \times 2 \times 7 \times 7$
pooling	Average Pooling	$512 \times 1 \times 1 \times 1$
flatten	–	512
dense	–	3